nature communications

Article

https://doi.org/10.1038/s41467-024-54726-9

The hyper-enrichment of silver through the aggregation of silver sulfide nanoparticles

Received: 20 December 2023

Accepted: 19 November 2024

Published online: 26 November 2024

Check for updates

Mingchun Chai[1,7] ✉, Anthony E. Williams-Jones[2], Wei Fu[1], Jianwei Li[3,4,7] ✉ & Cheng Xu[1,5,6]

Silver deposits have long been considered to form due to the direct precipitation of silver minerals from aqueous fluids, in which the metal is transported as chloride and/or bisulfide complexes. Ultra-high-grade silver ores have silver contents up to tens of weight-percent in the form of silver sulfides and native silver. Ore-forming fluids of most silver deposits, however, typically contain low silver contents of parts per million silver. The challenge is to explain how fluids with such low concentrations of silver can form ultra-high-grade silver ores. Here, we present direct mineralogical evidence from natural samples showing that the high-grade silver ores form from the aggregation of silver sulfide nanoparticles through intermediate microparticles and dendrites to acanthite crystals. Native silver grows from silver sulfides via solid-state silver ion aggregation. This study traces the formation of silver sulfides from their nanoparticulate precursors, thereby providing insights into the genesis of ultra-high-grade silver ores in a variety of metallogenic settings.

Silver commonly forms high-grade and, in some cases, ultra-high-grade ores in both hypogene and supergene environments[1–4]. The giant epithermal Imiter deposit contains ores with native silver weighing as much as 100 kg[1]. Comparable concentrations of silver have also been reported from the Chañarcillo deposit in Chile, as exemplified by a 20 t mass of silver halide plus native silver ore (75% silver)[2,5]. However, the concentration of silver in the fluids that form silver deposits ranges from parts per billion (ppb) to low parts per million (< 30 ppm) as determined from fluid inclusions[6]. Thus, it would take 10,000 tons of an ore fluid containing 10 ppm silver to form the 100 Kg sample referred to above, or a fluid-rock ratio of 1×10^5:1. How bonanza-grade silver ores can form from ore fluids with such low concentrations of silver remains unknown.

High-grade silver ores typically contain abundant silver dendrites and wires[2,7], which have been considered to precipitate from hydrothermal fluids that transport silver as chloride and/or bisulfide complexes (for reviews of hydrothermal silver speciation, see refs. 8,9). Although previous studies have provided evidence for the transport of gold as nanoparticles and used this evidence to explain the origin of bonanza gold deposits[10–12], to the best of our knowledge, this is not the case for silver. The gold nanoparticles are interpreted to occur in colloidal suspensions that are transported mechanically to the site of deposition[11,13–16], where they flocculate in response to a loss of surface charge induced by changes in pH or the introduction of an electrolyte[11,17]. The occurrence of silver-bearing electrum dendrites in epithermal Au-Ag deposits has been used as evidence of the transportation of electrum nanoparticles[18]. However, the role of these nanoparticles, if any, in the formation of silver dendrites (and wires) has not been evaluated. Although silver nanoparticles have been reported to be present in seafloor sulfide deposits[19], there is no direct evidence for the occurrence of silver sulfide nanoparticles in ore deposits, and the relationship of these nanoparticles to high-grade silver ores is thus unknown.

[1]College of Earth Sciences, Guilin University of Technology, Guilin, China. [2]Department of Earth and Planetary Sciences, McGill University, Montreal, QC, Canada. [3]State Key Laboratory of Geological Processes and Mineral Resources, China University of Geosciences, Wuhan, China. [4]School of Earth Resources, China University of Geosciences, Wuhan, China. [5]Key Laboratory of Orogenic Belts and Crustal Evolution, School of Earth and Space Sciences, Peking University, Beijing, China. [6]Collaborative Innovation Center for Exploration of Nonferrous Metal Deposits and Efficient Utilization of Resources by the Province and Ministry, Guilin University of Technology, Guilin, China. [7]These authors jointly supervised this work: Mingchun Chai and Jianwei Li.
✉e-mail: mcchai@cug.edu.cn; jwli@cug.edu.cn

Silver sulfide (acanthite, α-Ag_2S; argentite, β-Ag_2S) nanoparticles, as well as silver (native silver, Ag) nanoparticles and dendrites, and their hetero-dendrites (Ag-Ag_2S) have been synthesized in laboratory[20–22]. These syntheses have shown that nanoparticles are the basic building blocks for the formation of silver and silver sulfide dendrites and crystals[20]. They have also demonstrated that silver sulfide and silver nanoparticles can coexist to form hetero-nanoparticles (Ag_2S-Ag) and transition from one endmember to the other[21,23]. The synthesis of these nanoparticles and dendrites, therefore, provides a unique window through which to view the natural formation of silver sulfide and silver dendrites and crystals. Most importantly, they provide the basis for interpreting the characteristics of such structures in nature and for explaining the silver hyper-enrichment in some deposits.

The Poshan Ag-Pb-Zn deposit (2533 t silver at 243 g/t; ref. 24) in the Qinling orogen (central China; Fig. 1a) is an important example of the hyper-enrichment of silver that produces ores of acanthite and native silver. This deposit is located in the Tongbai area in the easternmost part of the Qinling orogen (Fig. 1b; ref. 25) that formed in successive orogenic cycles during the Paleozoic and Mesozoic eras[26,27]. The Poshan deposit is hosted by lower Paleozoic carbonaceous mica-quartz schist[28], and formed through the emplacement of orebodies in fractures that developed along the south flank of the Heqianzhuang anticline[24]. Two episodes of mineralization have been recognized based on the geology, the paragenesis and radiometric age determinations[24,29]. These comprise Early Cretaceous Ag-Pb-Zn mineralization and Late Miocene silver mineralization. The former is characterized by the occurrence of large numbers of quartz-carbonate-sulfide veins in carbonaceous mica-quartz schist containing galena, sphalerite, pyrite, chalcopyrite, arsenopyrite, freibergite [$(Ag, Cu, Fe, Zn)_{12}(Sb, As)_4S_{13}$], pyrargyrite [$Ag_3SbS_3$], and kustelite [Ag, Au], accompanied by gangue quartz, calcite, dolomite, ankerite, sericite, chlorite and apatite. An apatite U-Pb age of 125 ± 14 Ma was determined for this mineralization[24]. The Late Miocene mineralization occurs as 1 to 5 cm thick veins that cut the Early Cretaceous Ag-Pb-Zn orebodies and contains the assemblage calcite-chlorite-acanthite-native silver ± pyrite ± chalcopyrite ± galena ± quartz (Fig. 1c–e). Acanthite and native silver comprise the high-grade ores, which commonly have grades exceeding 1000 g/t silver and locally up to weight-percent levels of silver[29]. Silver wires are typically present if acanthite is

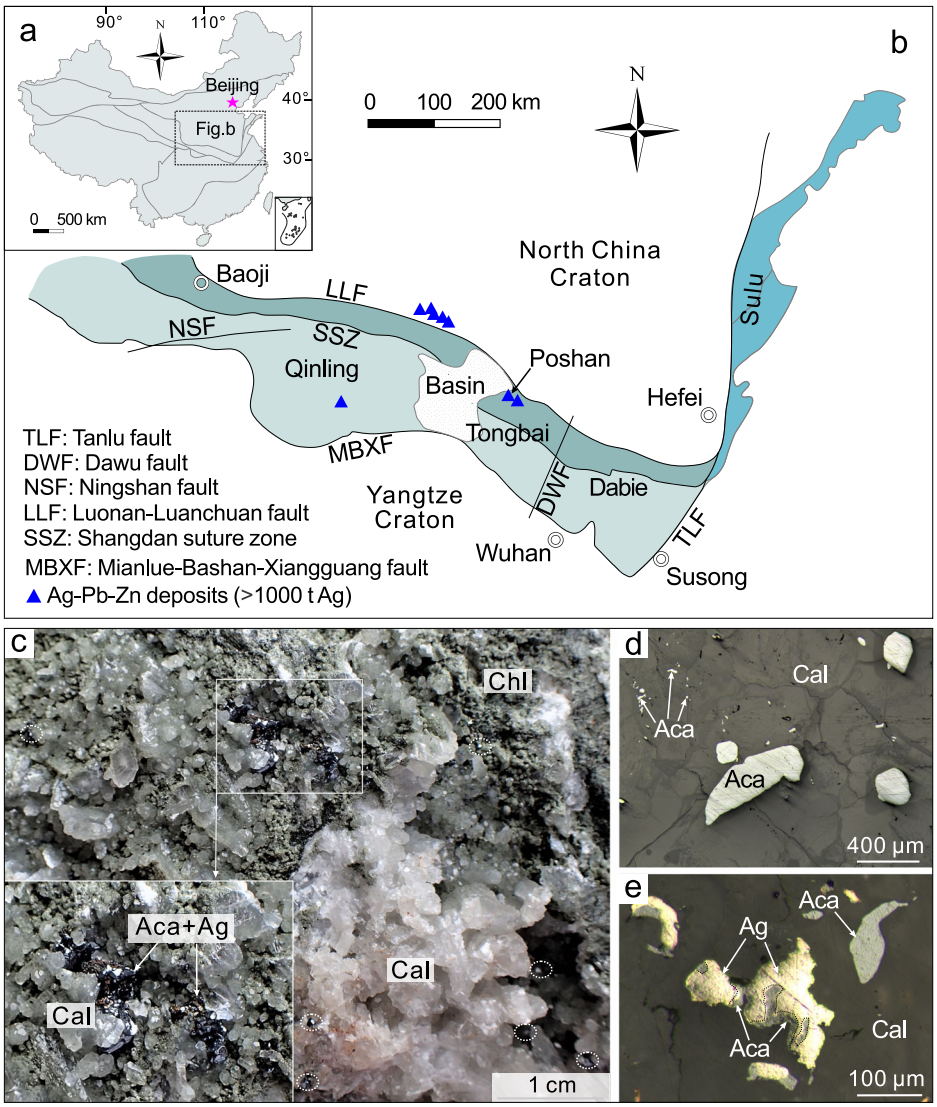

Fig. 1 | Location and the Late Miocene mineralization of the Poshan deposit. **a**, **b** Tectonic units of China (**a**) and the Qinling-Dabie orogen (**b**) showing the location of the Poshan Ag-Pb-Zn deposit (modified from Chai et al.[25]). **c** A photograph showing the occurrence of acanthite in the high-grade ores that contain abundant calcite and chlorite and variable proportions of acanthite and native silver. **d** Acanthite occurring both as anhedral crystals and tiny inclusions in calcite. **e** Native silver that replaced acanthite in calcite. Aca, acanthite; Ag, native silver; Cal, calcite; Chl, chlorite.

absent or scarce. Calcite from these high-grade ores yielded U-Pb ages of 8.6 Ma to 6.8 Ma[29]. On the basis of fluid inclusion analyses and stable isotope data (C-H-O-S), the fluids responsible for the Early Cretaceous mineralization were of magmatic-hydrothermal origin, had temperatures between 263 and 347°C and a salinity ≤ 5.1 wt% NaCl equivalent[24]. The fluids responsible for the Late Miocene mineralization were low-temperature (~130°C; estimated using the chlorite thermometer; ref. 29), but of unknown composition and source.

Here, we investigate the high-grade silver ores of the Late Miocene mineralization in the Poshan Ag-Pb-Zn deposit. Using scanning electron microscopy (SEM) and high-resolution transmission electron microscopy (HRTEM), we present evidence of the presence of silver sulfide nanoparticles and dendrites in the high-grade ores. These observations also revealed a crystallization sequence from silver sulfide nanoparticles to crystals and the transformation from dendritic silver sulfide to native silver. Our study provides direct evidence for the hypothesis that the aggregation of silver sulfide nanoparticles was the cause of the hyper-enrichment of silver in some deposits.

Results

Silver sulfide mineralogy

Scanning electron microscopic images reveal a variety of textures for silver sulfide (Ag_2S), including anhedral crystals, dendrites, microparticles, and nanoparticle aggregates (Fig. 2). Their composition and identity were established qualitatively by elemental mapping (Supplementary Fig. 1) and in situ micro X-ray diffraction (μXRD; Supplementary Fig. 2), respectively. The anhedral acanthite is associated with silver sulfide microparticles (~1 μm in diameter) that occur as self-organized clusters proximal to acanthite crystals (Fig. 2a). Silver sulfide submicroparticles form delicate dendrites, which are locally decorated with native silver (Fig. 2b). It is also noteworthy that the silver particles on these dendrites increased in size and number after exposure to a vacuum for a prolonged period of time (Fig. 2c). Silver dendrites, however, are not observed. Finally, silver sulfide nanoparticles and their aggregates are observed proximal to silver sulfide microparticles (Fig. 2d).

Silver sulfide nanoparticles

Transmitted electron microscopic images show that calcite hosts large numbers of silver sulfide nanoparticles with spherical to ellipsoidal shapes, ranging in diameter from several nanometers to a few tens of nanometers, with the majority of the particles in the size range of ~5–25 nm (Fig. 3). The silver sulfide nanoparticles are mostly isolated (Fig. 3a), although aggregates of nanoparticles are also observed (Fig. 3b). The d-spacings of the lattice fringes of the nanoparticles illustrated in Fig. 3c and Supplementary Fig. 3a–c vary from 0.222 nm to 0.251 nm. The silver sulfide composition of the nanoparticles was confirmed by energy-dispersive spectra and elemental mapping (Supplementary Fig. 3d–h). In combination with the electron diffraction patterns (Fig. 3d, e), these images confirm that the nanoparticles are now acanthite.

Discussion

The high-grade silver ores at Poshan contain large proportions of silver sulfide and native silver (Fig. 1c–e), which are intimately associated with calcite and chlorite. Calcite hosts numerous silver sulfide microparticles and nanoparticles (Figs. 1d, 2a, d, and 3a–c), raising the possibility that the silver sulfide may have crystallized from nanoparticles. The low temperature of the ore-forming fluid, as estimated using the chlorite geothermometer (~130 °C; ref. 29), is consistent with the silver sulfide being acanthite rather than argentite (acanthite is stable below ~177 °C; ref. 30; Supplementary Fig. 2). Therefore, the silver was most likely present as bisulfide complexes (e.g., $AgHS^0$) in the hydrothermal fluid at the temperature of the Late Miocene silver mineralization in the Poshan deposit, unless the pH and sulfur activity were exceptionally low or the oxygen fugacity was unusually high[8,9]. However, the low

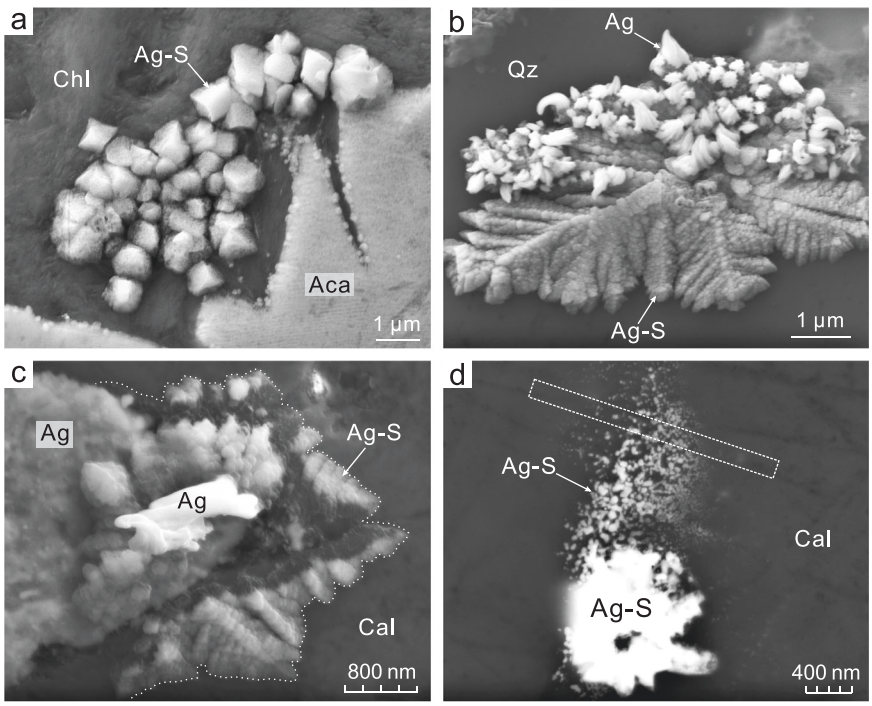

Fig. 2 | SEM images of silver sulfide and native silver in the high-grade ores. **a** Self-organized silver sulfide microparticle aggregates in association with anhedral acanthite. **b** Decoration of the surface of silver sulfide dendrites with nanoscale silver particles. **c** Growth of native silver accompanying the consumption of silver sulfide dendrites after ~65 minutes of exposure in a vacuum (<5×10^{-5} mbar) at 15 kV. **d** Coexistence of silver sulfide nanoparticles and their aggregates, with the rectangle illustrating the location of the TEM foil (not to scale). Note that the silver sulfides locally contain minor Cu and/or Fe. Aca, acanthite; Ag, native silver; Ag-S silver sulfide nanoparticles, microparticles or dendrites; Cal, calcite; Chl, chlorite; Qz, quartz.

https://doi.org/10.1038/s41467-024-54726-9

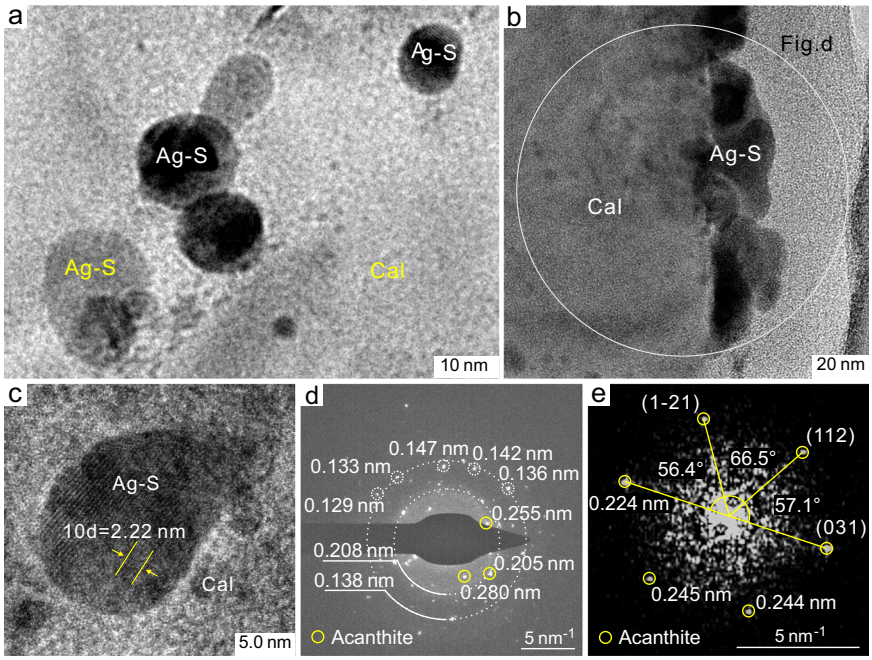

Fig. 3 | TEM images showing silver sulfide nanoparticles in calcite. a Spherical to ellipsoidal silver sulfide nanoparticles occurring as individuals or aggregates dispersed in calcite. **b** Aggregation of silver sulfide nanoparticles. **c** A representative silver sulfide nanoparticle exhibiting lattice fringes with a d-spacing of 0.222 nm. **d** An electron diffraction pattern for a selected area containing silver sulfide nanoparticles. **e** An electron diffraction pattern for the single silver sulfide nanoparticle illustrated in Supplementary Fig. 3b indicates that the silver sulfide is acanthite. Ag-S, silver sulfide nanoparticles; Cal, calcite.

concentration of silver in such hydrothermal fluids (< 30 ppm; ref. 6) makes it very unlikely that the Poshan bonanza ores, which have grades exceeding 1000 g/t silver and locally up to weight-percent levels of silver, could have formed by direct precipitation from these fluids.

The preservation of silver sulfide nanoparticles in the Poshan deposit (Figs. 2d and 3), suggests that instead of direct precipitation from a hydrothermal fluid, the acanthite crystallized from silver sulfide nanoparticles. To our knowledge, the only studies that have provided direct evidence of the mechanical transport of metal nanoparticles in hydrothermal fluids have been for gold and electrum[11,12,31]. Although silver sulfide nanoparticles have been synthesized in the laboratory[21], evidence for silver sulfide nanoparticles in natural samples has remained elusive. The occurrence of numerous spherical to ellipsoidal nanoparticles in the calcite of the Poshan deposit suggests strongly that silver sulfide nanoparticles were in suspension in the hydrothermal fluid during ore formation and were captured by the precipitated calcite (Fig. 3a). Therefore, based on the results of experiments and our mineralogical observations from the Poshan deposit, we propose that silver sulfide nanoparticles can be transported mechanically by hydrothermal fluids in a manner similar to that of gold and electrum nanoparticles[11,12,32]. The occurrence of silver nanoparticles in polymetallic sulfide ores[19], which deposited from a seafloor hydrothermal system, supports the hypothesis that this is also the case for silver sulfide in hydrothermal systems.

Our high-resolution TEM observations reveal that neighboring silver sulfide nanoparticles experienced aggregation during calcite precipitation (Figs. 2d and 3a), with individual nanoparticles flocculating to form colloidal aggregates (Fig. 4). This is consistent with the crystal growth theory of reorientation and aggregation[33,34], which posits that nanoparticles are the basic building blocks of crystals and the incipient expression of crystallization[18,20,35]. The aggregation is documented in this study by the occurrence of clusters of silver sulfide microparticles (~ 1 μm in diameter) adjacent to the crystalized acanthite (Fig. 2a). Additional evidence for aggregation is provided by the silver sulfide dendrites (Figs. 2b, 4 and Supplementary Fig. 1a–c), which we interpret to have developed as the result of the self-organization of the nano- to micro-particles. We consider that the dendrites represent an intermediate step in the development of crystals, and have been formed by oriented attachment or orthokinetic aggregation of individual particles (Figs. 2b and 4). Infilling of the spaces between the branches of the dendrites with nanoscale to microscale particles and further reorganization eventually led to the formation of acanthite with defined crystal shapes (Fig. 4). For an in-depth discussion of the process, readers are referred to Penn and Banfield[36] and Penn[37]. This study provides compelling evidence that hyper-enriched or high-grade silver sulfide ores do not form through direct hydrothermal precipitation. Instead, they are the products of the aggregation of silver sulfide nanoparticles.

The native silver in the Poshan deposit grows in the form of wires on the surface of calcite-chlorite assemblages or occurs as a replacement of acanthite within calcite (Fig. 1e). Silver particles were also observed to have decorated the surface of silver sulfide dendrites (Fig. 2b), indicating that the formation of elemental silver postdated the silver sulfide dendrites. We interpret the replacement of acanthite to have proceeded via the reaction as equation: $2Ag_2S + 2H_2O = 4Ag + 2H_2S + O_2$ (1). This reaction would have been driven to the right by reducing the activity of H_2S, potentially through its consumption in crystallizing the associated sulfide minerals (e.g., pyrite, chalcopyrite and galena). It is therefore, significant that where silver particles decorate silver sulfide dendrites, these particles increase in number and size with exposure of the sample to a vacuum for a prolonged period of time (Fig. 2c); the reaction in this case would have been expressed by the equation: $2Ag_2S = 4Ag + S_2$ (2). This reaction was likely facilitated by: 1) the generation of a thermoelectric gradient due to the irradiation of the acanthite, which broke the Ag-S bonds; 2) the application of an external electric field (SEM probe), which induced the transformation of nonconducting acanthite into conducting argentite and the formation of an ionic and electronic conductive channel[23]; and 3) a sharp decrease in the S_2 fugacity, because of the presence of a vacuum, which drove the reaction to the right. Mechanistically, the loss of sulfur would have induced solid-state silver ion aggregation due to the mobility of silver ions in the highly

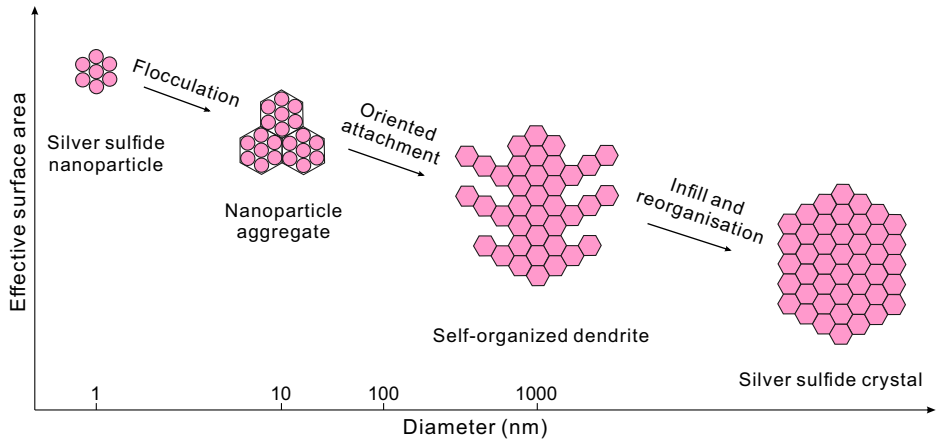

Fig. 4 | A schematic diagram illustrating the key processes of silver sulfide formation (modified from Saunders and Burke[31]). The formation of silver sulfide crystals initiates with the flocculation of silver sulfide nanoparticles to aggregates and microparticles, followed by an intermediate product of silver sulfide dendrites through self-assembly, oriented attachment of microparticles. Infilling the spaces between the branches of the dendrites with nanoscale to microscale particles and further reorganizing these particles that ultimately form silver sulfide with defined crystal shapes.

ion-conductive, sulfur-depleted silver-sulfide structure[38]. Thus, the dendritic-textured silver sulfide, i.e., the metastable acanthite precursor, would have promoted the formation of silver particles (Fig. 2b, c), microwires and eventually visible silver wires. In some natural settings, oxidation via the reaction expressed by the equation, $Ag_2S + O_2 = 2Ag + SO_2$ (3) may also lead to the production of silver from silver sulfide[39]. Formation of native silver by both reactions (1) and (3) is supported by our observation that silver wires are well-developed where acanthite is scarce and the observations of other researchers that silver wires commonly occur with acanthite (e.g., the Freiberg, Imiter, and Highland Bell deposits; ref. 40 and references therein). To summarize, we consider the native silver wires observed in this study to be the products of the transformation from silver sulfide rather than the direct deposition of silver from a hydrothermal fluid. The study provides mineralogical evidence for a centuries-old mystery of the natural formation of silver wires.

In conclusion, the mineralogical evidence presented here supports the hypothesis that the aggregation of silver sulfide nanoparticles is key to the formation of hyper-enriched silver ores from hydrothermal fluids. This process involves the flocculation of the nanoparticles and their self-assembly to form dendrites that are the precursors to the acanthite crystals. The growth of native silver wires from silver sulfide dendrites is consistent with the transformation of silver sulfide to elemental silver through the loss of sulfur and the solid-state aggregation of silver ions. This study provides insights into the formation of silver sulfide and native silver deposits and an enrichment process for high-grade silver ores.

Methods

Sample description

The high-grade silver ores investigated in this study represent the Late Miocene mineralization of the Poshan Ag-Pb-Zn deposit. The silver ores contain abundant calcite and chlorite, variable proportions of acanthite and native silver, and subordinate base metal sulfides (pyrite, chalcopyrite, and galena) and quartz (Fig. 1c–e). Acanthite usually presents as anhedral to subhedral crystals or tiny inclusions dispersed in calcite (Fig. 1d). Native silver occurs as wires growing on the surface of calcite aggregates or as a replacement of acanthite in calcite (Fig. 1e).

SEM analysis

Scanning electron microscopy was employed to characterize the morphology and texture of acanthite and native silver hosted in calcite. Secondary electron (SE) and back-scattered electron (BSE) images and elemental maps were acquired using a field emission scanning electron microscope (Σigma from Zeiss company) equipped with an energy dispersive spectrometer (EDS; X-Max 80 from Oxford company) at the Guangxi Key Laboratory of Hidden Metallic Ore Deposits Exploration, Guilin University of Technology. All the images were acquired under a vacuum of $<5 \times 10^{-5}$ mbar and an applied acceleration voltage of 15 kV.

In situ μXRD analysis

Micro X-ray diffraction spectra of silver sulfide crystals mounted in epoxy resin (2.5 cm mount) were recorded in situ using a microbeam diffractometer (Rigaku Dmax Rapid V, Cu Kα) at the Guangzhou Institute of Geochemistry, Chinese Academy of Sciences (GIGCAS). The analyses were conducted at 40 kV and 30 mA with a 100-μm collimator for a 100 s integration time. The sample stage was rotated with a fixed ω-axis (25°), and ϕ fluctuated from −80° to 20° (1° per second) to produce the maximum beam footprint on the investigated mineral. The diffraction spectra were characterized using the HighScore Plus software.

TEM analyses

Three electron-transparent foils (10 × 12 μm in size and ~100 nm in thickness) were prepared employing the focused ion beam (FIB) technique and SEM imaging at the Center for Lunar and Planetary Sciences, Institute of Geochemistry, Chinese Academy of Sciences (IGCAS). Transmission electron microscopy was used to characterize the morphology and textures of silver sulfide nanoparticles hosted in calcite. TEM and scanning TEM (STEM) imaging were performed using a Thermo Fisher Scientific FEI Talos F200S TEM with two windowless EDS detectors (FEI Super-X) at the Electron Microscopy Center of the GIGCAS. The analytical procedures and operating conditions were similar to those described in Xian et al.[41] and are briefly summarized here. An acceleration voltage of 200 kV was applied, and the TEM images were acquired using a Ceta 16 M camera. The images were analyzed using TEM image analysis (TIA) software supplied by Thermo Fisher Scientific. Selected area electron diffraction (SAED) patterns were recorded using a 10 μm selective area aperture (which produces a beam diameter of ~150 nm) in the microscope mode of the TEM system. The EDS spectra and elemental maps were acquired using a STEM system, thereby avoiding mass loss during data acquisition. Diffraction spectra for individual nanoparticles were acquired from high-resolution images using a Fast Fourier Transform (FFT) algorithm embedded in the TIA software.

Data availability

The data generated in this study have been deposited in the Figshare repository (https://doi.org/10.6084/m9.figshare.27262125). The raw data underlying the figures are available in the file Source Data. Source data are provided with this paper.

References

1. Cheilletz, A. et al. The giant Imiter silver deposit: Neoproterozoic epithermal mineralization in the Anti-Atlas, Morocco. *Miner. Depos.* **37**, 772–781 (2002).
2. Sillitoe, R. H. Hypogene reinterpretation of supergene silver enrichment at Chanarcillo, northern Chile. *Econ. Geol.* **102**, 777–781 (2007).
3. Sillitoe, R. H. Supergene silver enrichment reassessed. *Soc. Econ. Geol., Spec. Pub.* **14**, 15–32 (2009).
4. Burisch, M. et al. Genesis of hydrothermal silver-antimony-sulfide veins of the Bräunsdorf sector as part of the classic Freiberg silver mining district, Germany. *Miner. Depos.* **54**, 263–280 (2019).
5. Miller, B. L. & Singewald, J. T. *The Mineral Deposits of South America* (McGraw-Hill Book Company, New York, 1920).
6. Wilkinson, J. J. et al. How metalliferous brines line Mexican epithermal veins with silver. *Sci. Rep.* **3**, 2057 (2013).
7. Wallace, T. C. et al. Silver & silver-bearing minerals. *Rocks Miner.* **69**, 16–38 (1994).
8. Stefánsson, A. & Seward, T. M. Experimental determination of the stability and stoichiometry of sulphide complexes of silver(I) in hydrothermal solutions to 400 °C. *Geochim. Cosmochim. Acta* **67**, 1395–1413 (2003).
9. Williams-Jones, A. E. & Migdisov, A. A. Experimental constraints on the transport and deposition of metals in ore-forming hydrothermal systems. *Soc. Econ. Geol., Spec. Pub.* **18**, 77–95 (2014).
10. Saunders, J. A. Textural evidence of episodic introduction of metallic nanoparticles into bonanza epithermal ores. *Minerals* **2**, 228–243 (2012).
11. McLeish, D. F. et al. Colloidal transport and flocculation are the cause of the hyperenrichment of gold in nature. *Proc. Natl Acad. Sci.* **118**, e2100689118 (2021).
12. Petrella, L. et al. Nanoparticle suspensions from carbon-rich fluid make high-grade gold deposits. *Nat. Commun.* **13**, 3795 (2022).
13. Saunders, J. A. Colloidal transport of gold and silica in epithermal precious-metal systems: evidence from the Sleeper deposit, Nevada. *Geology* **18**, 757–760 (1990).
14. Herrington, R. J. & Wilkinson, J. J. Colloidal gold and silica in mesothermal vein systems. *Geology* **21**, 539–542 (1993).
15. Hannington, M. et al. Gold enrichment in active geothermal systems by accumulating colloidal suspensions. *Nat. Geosci.* **9**, 299–302 (2016).
16. Petrella, L. et al. Colloidal gold transport: a key to high-grade gold mineralization? *Miner. Depos.* **55**, 1247–1254 (2020).
17. McLeish, D. F. et al. Extreme shifts in pyrite sulfur isotope compositions reveal the path to bonanza gold. *Proc. Natl Acad. Sci.* **121**, e2402116121 (2024).
18. Saunders, J. A. et al. Scanning-electron-microscope imaging of gold (electrum) nanoparticles in middle Miocene bonanza epithermal ores from northern Nevada, USA. *Miner. Depos.* **55**, 389–398 (2020).
19. Wu, Z. W. et al. Occurrences and distribution of "invisible" precious metals in sulfide deposits from the Edmond hydrothermal field, Central Indian Ridge. *Ore Geol. Rev.* **79**, 105–132 (2016).
20. Zhou, Q. et al. Nanoparticle-based crystal growth via multistep self-assembly. *Crystengcomm* **15**, 5114–5118 (2013).
21. Sadovnikov, S. I. & Gusev, A. I. Recent progress in nanostructured silver sulfide: from synthesis and nonstoichiometry to properties. *J. Mater. Chem. A* **5**, 17676–17704 (2017).
22. Zhang, S. C. et al. Facile preparation of Ag-Ag_2S hetero-dendrites with high visible light photocatalytic activity. *J. Mater. Sci.* **53**, 6482–6493 (2018).
23. Xu, Z. et al. Real-time in situ HRTEM-resolved resistance switching of Ag_2S nanoscale ionic conductor. *ACS nano* **4**, 2515–2522 (2010).
24. Chai, M. C. et al. Precipitation of Ag-Pb-Zn ores of the Poshan vein deposit in the Qinling orogen (central China) by dilution of magmatic hydrothermal fluids. *Geol. Soc. Am. Bull.* **136**, 4072–4090 (2024).
25. Chai, M. C. et al. Paleozoic orogenic gold mineralization from metamorphism of volcanic sequences in the North Qinling terrane (central China): Insights from the Yindongpo gold deposit in the Tongbai area. *Miner. Depos.* **59**, 1531–1552 (2024).
26. Meng, Q. R. & Zhang, G. W. Timing of collision of the North and South China blocks: controversy and reconciliation. *Geology* **27**, 123–126 (1999).
27. Dong, Y. P. & Santosh, M. Tectonic architecture and multiple orogeny of the Qinling Orogenic Belt, Central China. *Gondwana Res* **29**, 1–40 (2016).
28. Zhang, J. et al. Lead isotope systematics of the Weishancheng Au-Ag belt, Tongbai Mountains, central China: implication for ore genesis. *Int. Geol. Rev.* **53**, 656–676 (2011).
29. Chai, M. C. *The Paleozoic-Mesozoic metallogenesis in the Tongbai area, central China*. China University of Geosciences, Wuhan (Ph.D. dissertation; in Chinese with English abstract), https://doi.org/10.27492/d.cnki.gzdzu.2021.000214 (2021).
30. Kracek, F. C. Phase relations in the system sulfur-silver and the transitions in silver sulfide. *Trans. Am. Geophys. Union* **27**, 364–374 (1946).
31. Saunders, J. & Burke, M. Formation and aggregation of gold (electrum) nanoparticles in epithermal ores. *Minerals* **7**, 163 (2017).
32. Hough, R. M. et al. Naturally occurring gold nanoparticles and nanoplates. *Geology* **36**, 571–574 (2008).
33. Banfield, J. F. et al. Aggregation-based crystal growth and microstructure development in natural iron oxyhydroxide biomineralization products. *Science* **289**, 751–754 (2000).
34. Theissmann, R. et al. Crystallographic reorientation and nanoparticle coalescence. *Phys. Rev. B* **78**, 205413 (2008).
35. Hochella, M. F. et al. Nanominerals, mineral nanoparticles, and earth systems. *Science* **319**, 1631–1635 (2008).
36. Penn, R. L. & Banfield, J. F. Imperfect oriented attachment: dislocation generation in defect-free nanocrystals. *Science* **281**, 969–971 (1998).
37. Penn, R. L. Kinetics of oriented aggregation. *J. Phys. Chem. B* **108**, 12707–12712 (2004).
38. Anderson, C. J. et al. Natural solid-state ion conduction induces metal isotope fractionation. *Geology* **47**, 617–621 (2019).
39. Boellinghaus, T. et al. Microstructural insights into natural silver wires. *Sci. Rep.* **8**, 9053–9059 (2018).
40. Anderson, C. J. & Rakovan, J. Connoisseur's choice: wire silver, Kongsberg, Norway & wire gold, Ground Hog Mine, Gilman, Colorado. *Rocks Miner.* **92**, 344–357 (2017).
41. Xian, H. Y. et al. Hyperenrichment of gold in pyrite induced by solid-state transportation. *Commun. Earth Environ.* **3**, 308 (2022).

Acknowledgements

M.C. acknowledges financial support from the National Natural Science Foundation of China (NSFC; No. 42202072). J.L. was funded by NSFC (No. 42321001 and 42130814). Yuan-Yun Wen (IGCAS), Jie-Yang Xie, Tian-Qi Zhang, Jing-Wen Zhou (GIGCAS), and Jie Wu (Guilin University of Technology) assisted with the laboratory analyses.

Author contributions

M.C. conceived and performed the research and wrote and revised the manuscript. A.E. W-J. helped interpret the data, commented on and

revised the manuscript, and polished the language. J.L. conceived and supervised the research and revised the manuscript. W.F. and C.X. discussed the results and contributed to data interpretation.

Competing interests
The authors declare no competing interests.

Additional information
Supplementary information The online version contains supplementary material available at https://doi.org/10.1038/s41467-024-54726-9.

Correspondence and requests for materials should be addressed to Mingchun Chai or Jianwei Li.

Peer review information *Nature Communications* thanks Denis Fougerouse, Stylianos Tombros, and the other, anonymous, reviewer(s) for their contribution to the peer review of this work. A peer review file is available.